Segmentation of the sternum from low-dose chest CT images

Shuang Liu*, Yiting Xie and Anthony P. Reeves
School of Electrical and Computer Engineering, Cornell University, Ithaca, NY, USA

ABSTRACT

Segmentation of the sternum in medical images is of clinical significance as it frequently serves as a stable reference to image registration and segmentation of other organs in the chest region. In this paper we present a fully automated algorithm to segment the sternum in low-dose chest CT images (LDCT). The proposed algorithm first locates an axial seed slice and then segments the sternum cross section on the seed slice by matching a rectangle model. Furthermore, it tracks and segments the complete sternum in the cranial and caudal direction respectively through sequential axial slices starting from the seed slice. The cross section on each axial slice is segmented using score functions that are designed to have local maxima at the boundaries of the sternum. Finally, the sternal angle is localized. The algorithm is designed to be specifically robust with respect to cartilage calcifications and to accommodate the high noise levels encountered with LDCT images. Segmentation of 351 cases from public datasets was evaluated visually with only 1 failing to produce a usable segmentation. 87.2% of the 351 images have *good* segmentation and 12.5% have *acceptable* segmentation. The sternal body segmentation and the localization of the sternal angle and the vertical extents of the sternum were also evaluated quantitatively for 25 *good* cases and 25 *acceptable* cases. The overall weighted mean DC of 0.897 and weighted mean distance error of 2.88 mm demonstrate that the algorithm achieves encouraging performance in both segmenting the sternal body and localizing the sternal angle.

Keywords: Sternum segmentation, low-dose CT images, fully automated segmentation

1. INTRODUCTION

The sternum is a bony structure located in the medial and anterior thoracic cavity, and it consists of three main parts as shown in Figure 1: the manubrium, the body of sternum and the xiphoid process. A reliable sternum segmentation in medical images is of clinical significance due to the fact that sternum frequently serves as a stable reference to image registration and segmentation of other organs in the chest region such as lung [1], heart [2] and breast [3]. Furthermore, the sternal angle A shown in Figure 1(b), is considered a major anatomical landmark [4] because it is located in the horizontal plane that has been used to locate the carina, the aorta arch, the superior limit of pericardium and the separation between superior mediastinum and inferior mediastinum.
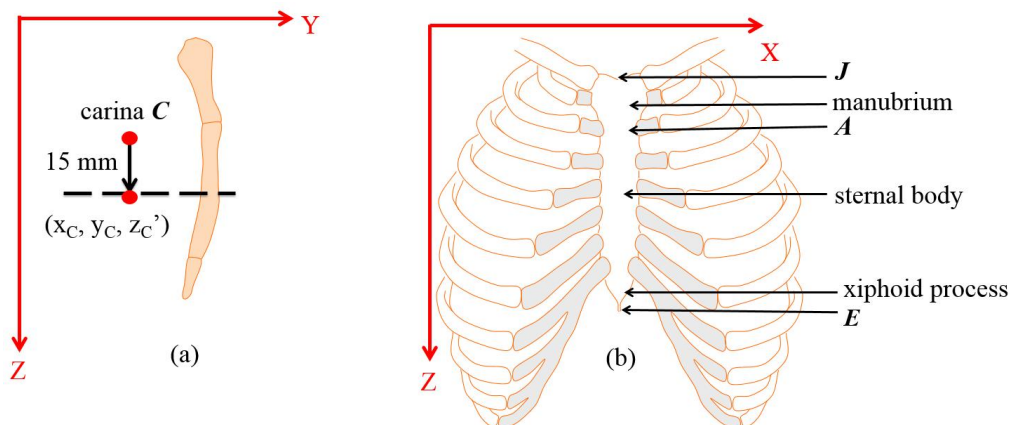
Figure 1. The (a) sagittal and (b) coronal view of a sternum. (x_C, y_C, z_C') is obtained by projecting the carina C (x_C, y_C, z_C) in the caudal direction for 15 mm .

A fully automated algorithm to segment the sternum and to localize the sternal angle in LDCT is presented in this paper. The two main challenges to be addressed are the high noise levels present in the low-dose scans and possible calcifications that may be confused as the sternum in the costal cartilage adjacent to the sternum. For cases in which the sternum is the only calcified structure in the anterior region of the thorax as shown in Figure 2(a, b), segmentation may be accomplished by simply thresholding for high intensity calcium. However, this will not work for cases shown in Figure 2(c, d) which contain significant additional cartilage calcifications in the costal region.
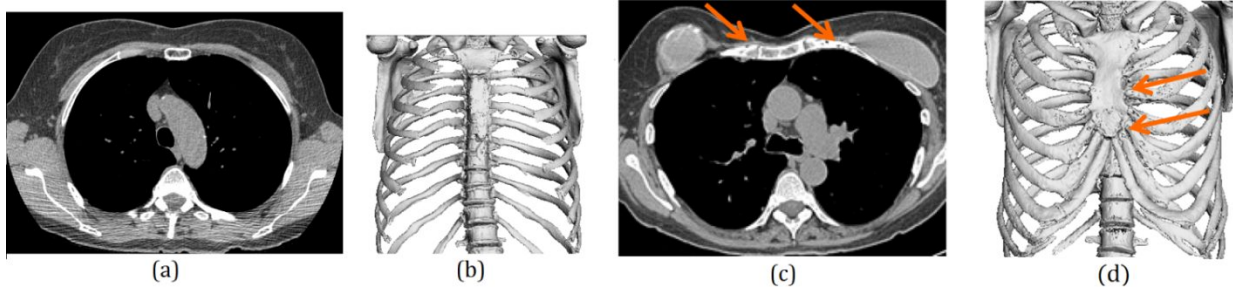

Figure 2. (a) CT axial image and (b) 3D coronal visualization of high intensity regions in a case with no significant rib cartilage calcification. (c) CT axial image and (d) 3D coronal visualization of high intensity regions in a case with extensive rib cartilage calcification as indicated by arrows.

There has been very detailed work on sternum reported in the literature especially in the context of low-dose CT images. Sternum segmentation has been mentioned briefly in papers centered on the heart[2], lung[1] and breast[3], however, in these studies no evaluations on sternum segmentation have been performed. Pazokifard et al developed and evaluated a fully automated algorithm[5] for the segmentation of sternum on 16 CT images taken for various clinical indications. Their method first projected 3D images into 2D coronal planes, and then segmented the sternum based on 2D active contour algorithm.

2. ALGORITHM

The presented algorithm was constructed upon the airway and rib segmentation developed in our previous work[6, 7], and consisted of the following 5 steps as shown in Figure 3:

1. Extract the region of interest (ROI).
2. Locate an axial seed slice z_S that intersects the sternal body in an intercostal space.
3. Segment the axial cross section of the sternum on the seed slice z_S.
4. Track and segment the sternum in the cranial and caudal direction respectively through sequential axial image slices starting from the sternum cross section on z_S.
5. Locate the axial level of sternal angle A.
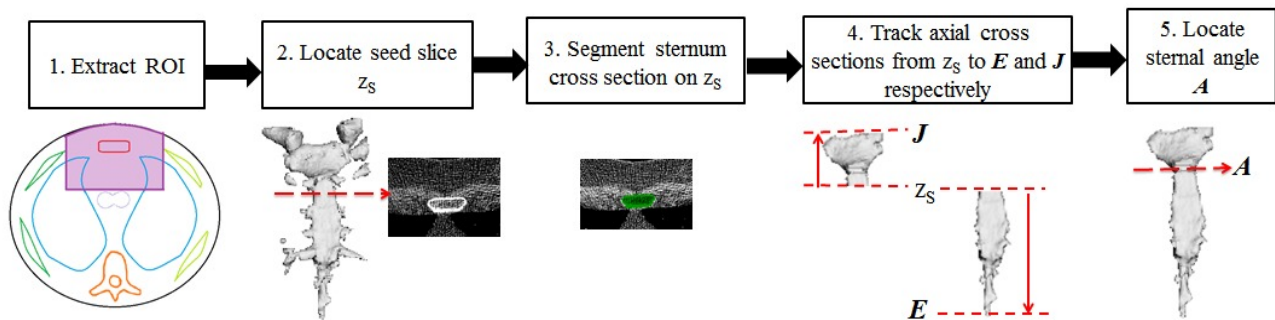
Figure 3. Sternum segmentation flow chart.

2.1 ROI extraction

The sternum is located between the ribs and anteriorly to the airway. The presented algorithm is only applied to the sternum ROI, which is obtained by extracting the region that is bounded posteriorly by the airway and laterally by the ribs as shown in Figure 4. The airway and ribs on the input CT images are segmented using methods presented in our previous work[6, 7].
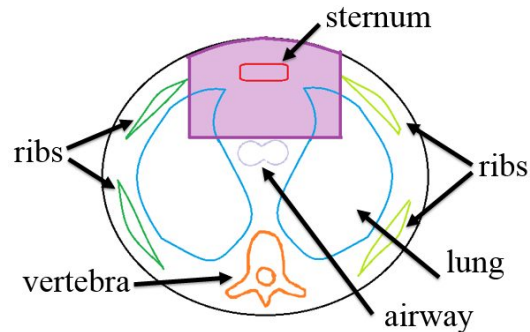
Figure 4. The ROI of sternum shown in shaded region on an axial slice

2.2 Axial seed slice z_S selection

An axial slice is selected as the seed slice z_S to serve as a robust starting point for the later tracking of the whole sternum. To facilitate the subsequent segmentation, the seed slice is required to contain few calcified rib cartilages and be located within the sternal body due to the following two points of considerations: First, the long extent and regular rectangular cross section of the sternal body provide robust features; Second, significant additional cartilage calcifications as in Figure 2(c, d) complicate the determination of sternum boundaries, especially lateral boundaries.
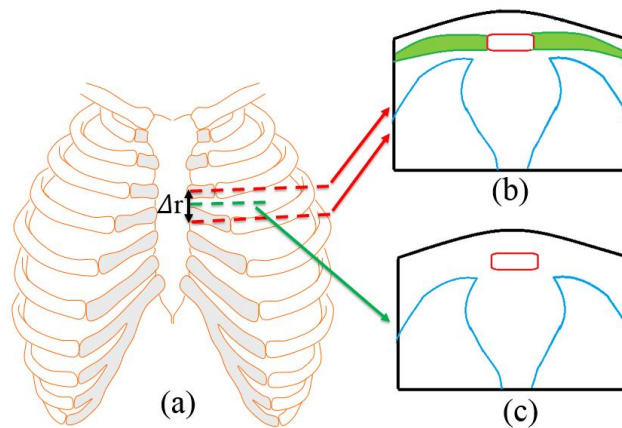
Figure 5. (a) Δr is used to approximate one intercostal distance. The ROI in axial view (b) in the costal region and (c) in an intercostal region.

The seed slice z_S is determined by two steps:

1. Locate an axial slice z_C'of the sternal body by projecting the carina $\boldsymbol{C}$ inferiorly for 15 mm as shown in Figure 1 (a).
2. Select the axial slice with the minimal lateral range of calcified voxels (voxels with image intensity $> \varepsilon_1$) among all axial slices in a vertical span of Δr surrounding z_C'. Δr is pre-defined empirically and used to approximate one intercostal distance as shown in Figure 5(a).

The location of carina $\boldsymbol{C}$ is provided by the airway segmentation and is considered to be located at approximately the same axial level as the sternal angle $\boldsymbol{A}$ [4]. Using 3D Cartesian coordinate system as shown in Figure 1, and (x_C, y_C, z_C) to denote the coordinates of the carina, $z_C' = z_C + 15mm$.

The rib cartilages are located in the costal regions as shown in Figure 5. Therefore, even for scans with severe cartilage calcifications, the seed slice z_S with few calcified cartilages can be determined in an intercostal space, i.e., within the vertical span of one costal distance Δr surrounding z_C'.

2.3 Segmentation of the axial cross section on z_S

The axial cross section of the sternum on the seed slice z_S is segmented by fitting a rectangle that is aligned with the coordinate system established as in Figure 1. The anterior ($y = y_A$) and posterior ($y = y_P$) sides of the rectangle are first determined by identifying two lines with the maximal scores among all lines that are parallel to the x-axis. Next, based on the distribution of calcifications at the anterior and posterior sides, the left ($x = x_L$) and right ($x = x_R$) sides of the rectangle are determined similarly using a score function. The posterior and anterior sides are determined first and serve as a reference for the detection of lateral sides because there are few calcifications that can be confused with the sternum in the anterior-posterior direction, while the calcified rib cartilages in the medial-lateral direction may be difficult to be distinguished from the sternum. The fitting rectangle is illustrated in Figure 6.
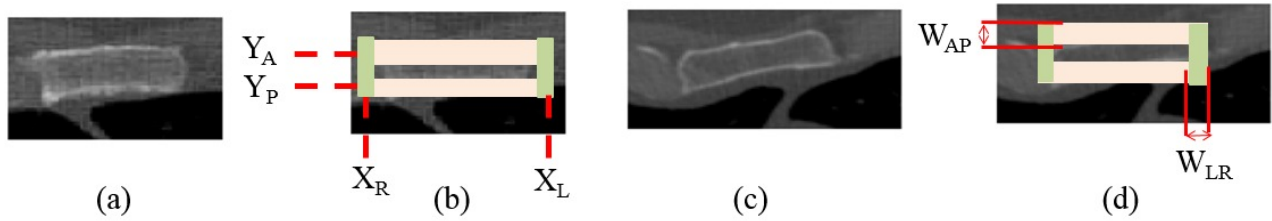

Figure 6. (a) (c) Axial cross section of the sternum and their corresponding fitting rectangles (b)(d).
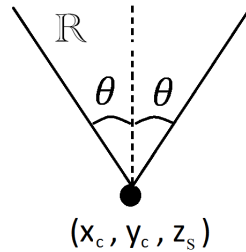

Figure 7. The illustration of region R, which is used to constrain the location of the sternum.

Two score functions, $S_{AP}(y)$ and $S_{LR}(x)$, are designed to have local maxima at the boundaries of the sternum and therefore are used to determine x_R, x_L, y_P and y_A. Since the boundaries of sternum are located at the transitions from the high intensity to low intensity in the medial region of human chest as shown in Figure 6 (a, c), both intensity information $S_I(I)$ and position information $S_G(d, \mu, \sigma)$ are incorporated into the definition of score functions. The region R is used to approximate the medial region of the chest and defined as the region bounded by two rays emanating from (x_C, y_C, z_S) at an angle θ from the y-axis as shown in Figure 7, where x_C and y_C are the coordinates of the carina C. If we let $I(\vec{P})$ denote the image intensity of voxel $\vec{P}$ with coordinates (p_X, p_Y, z_S), and let $dtr(\vec{P})$ denote the lateral distance from $\vec{P}$ to the region R, $S_{AP}(y)$, which measures the likelihood of a y coordinate to be y_P or y_A, is defined as follows:

$$S_{AP}(y) = \sum_{|p_Y - y| < 0.5 * W_{AP}} B_{AP}(\vec{P}, \varepsilon_1) * S_I(I(\vec{P})) * S_G(dtr(\vec{P}), 0, \sigma_R) \tag{1.1}$$

$$B_{AP}(\vec{P}, \varepsilon) = \begin{cases} 1, & \text{if } I(p_X, p_Y) > \varepsilon, \ I(p_X, p_Y +1) < \varepsilon \text{ or } I(p_X, p_Y -1) < \varepsilon \\ \\ 0, & \text{otherwise} \end{cases} \tag{1.2}$$

$$\begin{cases} 0, & \text{if } I < \varepsilon_1 \end{cases}$$

$$S_I(\text{I}) = \quad a * \text{I} + b, \qquad \text{if } \varepsilon_1 < \text{I} < \varepsilon_2 \tag{1.3}$$
$$1, \qquad\qquad \text{if I} > \varepsilon_2$$

$$S_G(\text{d}, \mu, \sigma) = e^{-\frac{(d-\mu)^2}{2\sigma^2}}, \qquad\qquad \text{for } \text{d} >= 0 \tag{1.4}$$

Where ε_1 and ε_2 are intensity thresholds for calcifications, a and b are the parameters of the piecewise linear function $S_I(\text{I})$, σ_R is the parameter associated with the penalty for voxels far away from the medial region $\boldsymbol{R}$, and $B_{AP}(\vec{P})$ is a characteristic function of voxels located at the transitions from high intensity to low intensity along y-axis, i.e., it has non-zero value only if $\vec{P}$ is calcified and has at least one non-calcified anterior or posterior neighbor.

The intensity component $S_I(\text{I})$ is a piecewise linear function of voxel intensity and assumes the follows: (1). If $I(\vec{P}) < \varepsilon_1$, $\vec{P}$ cannot be calcified; (2). If $I(\vec{P}) \geq \varepsilon_2$, $\vec{P}$ must be calcified; (3). If $\varepsilon_1 < I(\vec{P}) < \varepsilon_2$, the probability that $\vec{P}$ is calcified increases with $I(\vec{P})$. Binary thresholding is not used because it is not able to accommodate the large variations of bone densities and noise levels. (However, once the axial cross section is segmented, a reliable threshold value ε for the input image can then be decided by adaptive thresholding within the segmented cross section on z_S and be used for the remainder of the algorithm.)

The position component $S_G(\text{d}, \mu, \sigma)$ is a Gaussian function of voxel location d, where μ and σ are used to specify the location and width of the peak, respectively. The parameters μ and σ are decided based on empirical observations of the dimensions of the sternum and the prior knowledge that the sternum is more likely to be located in the medial part of human chest.

When considering a candidate coordinate y, all voxels located in the band with width of W_{AP} are used to calculate the score as defined in (1.1) and illustrated in Figure 6 (d). The width is introduced to accommodate cases as illustrated by Figure 6(c, d), where the actual sternum boundaries are not aligned with the coordinate axes due to the following two main reasons: First, the human body and the CT scanner may not be aligned exactly; Second, the axial cross sections of the sternum manubrium and xiphoid process are irregular and not modeled very well by a simple rectangle.

Similarly, $S_{LR}(x)$ that measures the likelihood of an x coordinate to be x_R or x_L is defined as follows:

$$S_{LR}(x) = \sum_{y_P < p_Y < y_A, |X - x| < 0.5 * W_{LR}} B_{LR}(\vec{P}, \varepsilon_1) * S_I\left(\text{I}(\vec{P})\right) * S_G\left(|p_X - x_S|, \mu_x, \sigma_x\right) \tag{2.1}$$

$$B_{LR}(\vec{P}, \varepsilon) = \begin{cases} 1, & \text{if } I(p_X, p_Y) > \varepsilon, \ I(p_X + 1, p_Y) < \varepsilon \text{ or } I(p_X - 1, p_Y) < \varepsilon \\ \\ 0, & \text{otherwise} \end{cases} \tag{2.2}$$

Where $B_{LR}(\vec{P})$ is the characteristic function of voxels located at the transitions from high intensity to low intensity along x-axis, and μ_x and σ_x are pre-defined parameters based on the empirical observations of the lateral extents of the sternum. The position component $S_G(|p_x - x_s|, \mu_x, \sigma_x)$ is defined using the center of mass (x_S, y_S) of calcified voxels at $y = y_P$ and $y = y_A$ as a reference for the determination of the lateral boundaries of the sternum. A calcified voxel (x, y) at $y = y_P$ or $y = y_A$ is used to calculate (x_S, y_S) only if it satisfies the following criteria: (1). If $y = y_A$, (x, y_P) is calcified; (2). If $y = y_P$, (x, y_A) is calcified. These rules help avoid calcified cartilage voxels because they might share either the same anterior or posterior boundary with the sternum, but it's less likely that they share both the same boundaries.

The two y coordinates that produce the most prominent local maxima of $T_{AP}(y)$ are selected to be y_P and y_A based on the relation $y_P < y_A$. Similarly, the two x coordinates that produce the most prominent local maxima of $T_{LR}(x)$ are selected to be x_R and x_L based on the relation $x_R < x_L$. Once the rectangle bounded by $y = y_P$, $y = y_A$, $x = x_R$ and $x = x_L$ is identified, the boundary of the sternum is determined by identifying the most exterior calcified voxels within the bounded region, and the resulting interior region is considered as the axial cross section of the sternum.

2.4 Segmentation based on the tracking in the cranial and caudal direction

The segmentation of the whole sternum is accomplished by tracking sternum cross sections starting from z_S in the cranial and caudal direction respectively through sequential axial slices. The cross section on each axial slice z is segmented using a method similar to that described in the previous section based on a rectangle model and score functions, F_{AP} (y, z) and F_{LR}(x, z), with additional prior knowledge about the sternum segmented previously. For the tracking in the cranial direction, the score functions are defined for each $z < z_S$ as follows:

$$F_{AP} (y, z) = \sum_{|p_Y - y| < 0.5 * W_{AP}} B_{AP}(\vec{P},\ \varepsilon) * S_G(|p_x - x_s(Z_P)|, 0, \sigma_y) \tag{3}$$

$$F_{LR} (x, z) = \sum_{y_P(Z_P) < p_Y < y_A(Z_P), |p_x - x| < 0.5 * W_{LR}} B_{LR}(\vec{P},\ \varepsilon) * S_G(|p_x - x_s(Z_P)|, \mu_x, \sigma_x) \tag{4}$$

$$x_S(Z_P) = (x_R(Z_P) + x_L(Z_P))\ /\ 2 \tag{5}$$

Where (p_x, p_y, z) is the coordinate of voxel $\vec{P}$ on axial slice z, Z_P is the previous slice, i.e. $Z_P = z + 1$, and $x_S(Z_P)$ is the estimated x coordinate of the center of the cross section on z.

The parameters used in the position weight S_G (i.e., μ_x, σ_x and σ_y) are pre-defined based on the empirical observations of the lateral extents of the sternum. The width of the sides of the rectangle model (i.e., W_{LR} and W_{AP}) is also pre-defined according to the usual greatest orientation of patient body with respect to the scanner axes. This set of parameters takes different values for the manubrium and the rest of the sternum because there is a significant increase of axial dimensions and shape irregularity for the manubrium compared to the rest of the sternum. As a result, when tracking in the cranial direction, the lateral extent of segmented sternum on each axial slice is checked to see if it exceeds a pre-defined width X_M, which suggesting that the manubrium is reached and the parameters for the manubrium will be used for subsequent tracking.

The position components S_G used in (3) and (4) assume that the cross section on z centered at $x_S(Z_P)$ laterally, and voxels located far away (with respect to the dimensions of the sternum) from the center are unlikely to belong to the sternum boundary. The determined left side $x_L(Z_P)$ and right side $x_R(Z_P)$ of the fitting rectangle on Z_P are used to estimate the lateral center on z as defined in (5), because sternum cross sections on consecutive axial slices are connected and has similar dimensions.

The tracking in the cranial direction is summarized as follows:

1. Starting from the axial slice $z = z_S - 1$
2. Calculate F_{AP} (y, z) and determine $y_P(z)$ and $y_A(z)$ by finding the two most prominent local maxima.
3. Calculate F_{LR} (x, z) and determine $x_R(z)$ and $x_L(z)$ by finding the two most prominent local maxima.
4. Apply 2D connected component labelling on the calcified voxels within the bounded region. Components intersecting $x = x_S(z)$ are considered as sternum exterior boundaries, thus the region enclosed by the boundary is considered as the sternum cross section on z .
5. Check the lateral extent of segmented cross section to see if the manubrium is reached. If so, parameters for the manubrium will be used for the subsequent tracking.
6. Move to next slice $z = z - 1$, repeat step 2 to 5 until there are no calcified voxels intersecting $x = x_S(z + 1)$.

For the tracking in the cranial direction, a similar method to that was summarized above is used with the following two modifications:

1. The tracking direction is reversed, thus, the previous slice $Z_P = z - 1$.
2. The same set of parameters is used for all slices, i.e., there is no need to check if the manubrium is reached.

2.5 Sternal angle *A* localization

The sternal angle *A* is generally located at the axial level with significant changes of lateral extents and y coordinates along z-axis as shown in Figure 1. Given the segmented sternum, the axial level of *A* is determined as follows:

1. For each axial slice $z < Z_S$, compute the slope S_X (z) of lateral extent of the segmented cross section on z.
2. For each axial slice $z < Z_S$, compute the slope S_Y (z) of y coordinates of the center of the segmented cross section on z.
3. Among all axial slices $z < Z_S$, locate the axial level z with the greatest S_X (z) + S_Y (z), which corresponds to the most significant changes of the lateral extents and locations in the anterior-posterior direction.

3. EXPERIMENTS

The presented algorithm was applied on 351 LDCT images (120kV-140kV, 40mA- 80mA) from VIA-ELCAP [8] and LIDC [9] public datasets. Both visual inspection and quantitative evaluation were used to validate the results. For the visual inspection, the 3D sternum segmentation were compared with calcified regions segmented based on our previous work[7] in both coronal and sagittal view, as shown in Figure 8 (a, d, e, f). The results were categorized into *good*, *acceptable*, and *not acceptable*. *Good* segmentation is required to terminate approximately at the jugular notch *J* and *E* (the cranial end of the sternum) and include the complete sternal body and no calcified cartilage, as shown in Figure 9. *Acceptable* segmentation allows minor errors at termination, however, it must include the majority of the sternal body and no significant amount of calcified cartilage, as shown in Figure 10.

For the quantitative evaluation, the segmentation of the sternal body and the localization of *J*, *A* and *E* were compared with the ground truth manually for 25 randomly selected *good* cases and 25 randomly selected *acceptable* cases. For each of the 50 cases, the sternal body was first divided uniformly into 6 segments in the vertical direction as shown in Figure 8 (a). On each of the 5 resulting intermediate dividing axial slices, the exterior boundary of the sternum cross section was manually annotated as shown in Figure 8 (b), and the resulting interior region was used as the ground truth for the cross section segmentation. The dice coefficient (DC) was used to measure the agreement between the ground truth and the segmentation of the sternal body. The axial levels of *J*, *A* and *E* were also manually identified as shown in Figure 8 (c) and used as the ground truth to calculate the distance error with respect to the location reported by the algorithm.
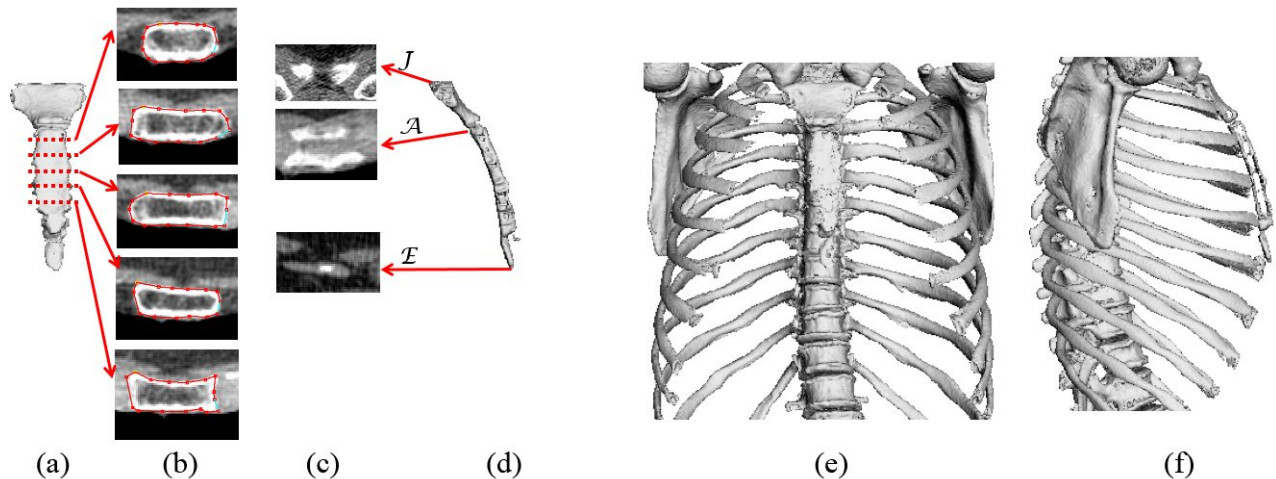

Figure 8. Visual and quantitative evaluation methods. (a, d, e, f) are used for visual inspection. (b, c) show the ground truth annotated manually. The 3D visualizations of the sternum segmentation are shown in (a) coronal view and the (d) sagittal view. Calcified regions ((e) coronal view and (f) sagittal view) are used as reference for the qualitative (visual) evaluation.
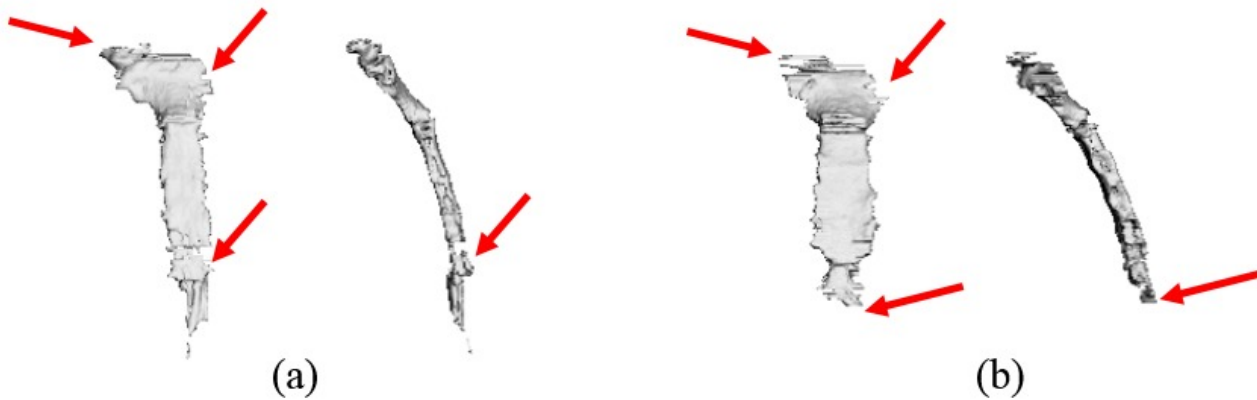
4. RESULTS

From the visual inspection, 87.2% of the 351 images achieve *good* segmentation and 12.5% achieve *acceptable* segmentation). Only 1 case has *not acceptable* segmentation. Three examples of *good* segmentation are shown in Figure 9 and two examples of *acceptable* segmentation are shown in Figure 10.
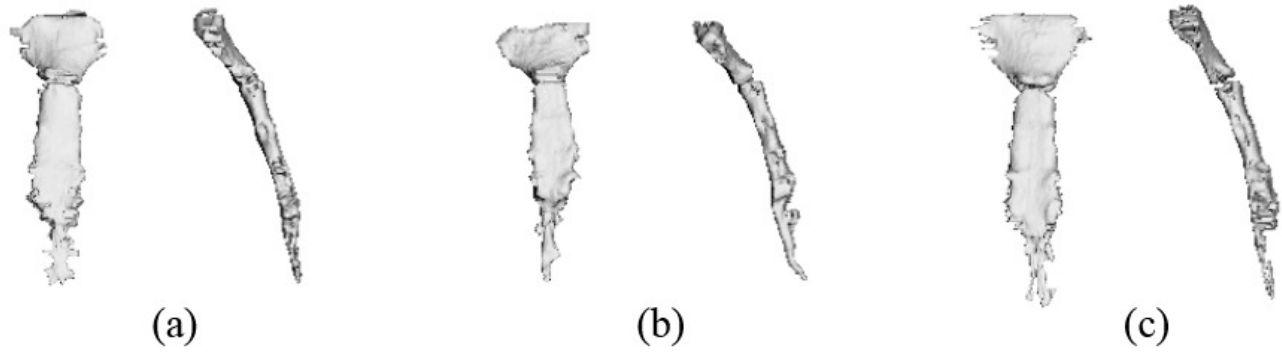
Figure 9. Three examples of segmentation results that have been categorized as *good* by visual evaluation.

Figure 10. Two examples of segmentation results that have been categorized as *acceptable* by visual evaluation. The location with issues are marked by arrows.

Table 1. Quantitative evaluation results for 25 randomly selected good cases and 25 randomly selected acceptable cases: mean distance error (MDE) to **J**, **A** and **E**, mean Dice coefficient for sternal body segmentation (MDC), and their respective standard deviation σ. The overall performance on the last row is the weighted combination of good (with weight of 0.875) and acceptable (with weight of 0.125) results.

	MDE to J (mm)	σ (J)	MDE to A (mm)	σ (A)	MDE to E (mm)	σ (E)	MDC	σ (DC)
Good	2.11	2.83	2.52	4.07	2.18	3.32	0.905	0.021
Acceptable	5.74	6.46	5.41	9.45	11.9	14.9	0.840	0.104
Overall	2.56	3.28	2.88	4.74	3.39	4.77	0.897	0.031

For the quantitative evaluation, the results of the 50 cases are summarized in Table 1. The overall weight performance is calculated by assigning weight of 0.875 to *goo*d cases and weight of 0.125 to *acceptable* cases according to the percentage of the number of cases in each category based on the visual inspection results. The overall mean DC for the sternal body segmentation is 0.897 with standard deviation of 0.031, and the mean distance error for the sternal angle localization is 2.88 mm with standard deviation of 4.74.

5. DISCUSSION

The quantitative evaluation shows that the algorithm achieves high mean DC of 0.905 for the sternal body segmentation and small distance error of less than 3 mm for localizing the sternal angle and vertical extents for the *good* cases (accounting for 87.2% of the total 351 images). The performance of *acceptable* cases is not as promising as that of *good* cases but the outcomes are still useful. The major issues are the incomplete manubrium and the inclusion of clavicles as indicated in Figure 10, thereby resulting in large distance error for locating the superior end of the sternum. This issue usually results from high levels of noise around the superior part of the manubrium in low-dose CT images due to surrounding (shoulder) bone structures. Another issue occurs for some acceptable cases is that the xiphoid process is not completely segmented as shown in Figure 10 (b), which is mainly caused by the irregularity of the shape and the large individual variations of dimensions of the xiphoid process, suggesting that a rectangle model may not fit the axial cross sections of the xiphoid process very well.

Only one case fails to obtain useful segmentation due to the failure occurs in the stage of selecting a seed slice in the intercostal space. For this *not acceptable* case, the angle between the human body and the scanner axis is approximately 5.9° as illustrated in Figure 11 (a). As a result, no axial slice can be found to be located in the intercostal space completely because if the left side of the body belongs to the intercostal space as shown in Figure 11 (b), the right side belongs to the costal space. The algorithm selects the axial slice shown in Figure 11 (b) as the seed slice for this *not acceptable* case. Since there are significant cartilage calcifications on the seed slice, the subsequent segmentation of cross sections is performed unsuccessfully.
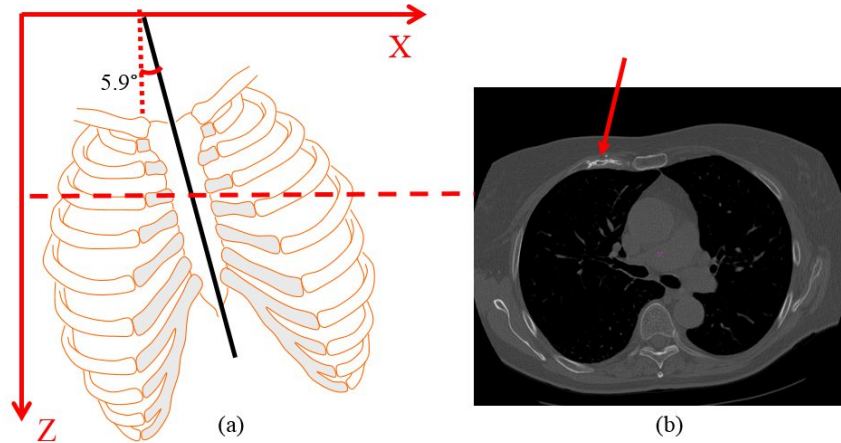
Figure 11. The illustration of the situation (the *not acceptable* case) that the human body is not aligned with scanner.

The presented algorithm is designed to be specifically robust with respect to cartilage calcifications and to accommodate the high noise levels encountered with LDCT images. Human anatomy is utilized to guide the initialization of the sternum tracking by selecting a seed slice from the intercostal space to avoid the cartilage calcifications. The score functions used to fit rectangle model for axial cross sections take account of not only the image information of the current slice but also the segmentation results on axial levels that have been tracked through, which improves the robustness of the algorithm with respect to the noise on the current axial level.

For the future work, we plan to improve the algorithm in two aspects. First, a better fitting model should be proposed for axial cross sections of the manubrium and xiphoid process. Second, the orientation of the human body with respect to the scanner can be determined first and then used as additional input information for the segmentation algorithm.

6. CONCLUSION

A fully automated algorithm to segment the sternum and to localize the sternal angle in LDCT was presented in this paper. Segmentation of 351 cases was evaluated visually with only 1 failing to produce a usable segmentation. Quantitative evaluation on 50 LDCT images also demonstrates that the algorithm achieves encouraging performance in

segmenting the sternal body and localizing the sternal angle, resulting in a weighted mean DC of 0.897 and a weighted mean distance error of 2.88 mm, respectively.

ACKNOWLEDGMENTS

REFERENCES

[1] Betke, M., Hong, H., Thomas, D., Prince, C., et al., "Landmark detection in the chest and registration of lung surfaces with an application to nodule registration," Medical Image Analysis 7(3), 265-281 (2003).

[2] Zheng, Y., Vega-Higuera, F., Zhou, S. K. and Comaniciu, D., "Fast and automatic heart isolation in 3D CT volumes: Optimal shape initialization," Machine Learning in Medical Imaging, 84-91 (2010).

[3] Reed, V. K., Woodward, W. A., Zhang, L., Strom, E. A., et al., "Automatic segmentation of whole breast using atlas approach and deformable image registration," International journal of radiation oncology, biology, physics 73(5), 1493-1500 (2009).

[4] Selthofer, R., Nikolić, V., Mrčela, T., Radić, R., et al., "Morphometric analysis of the sternum," Collegium antropologicum 30(1), 43-47 (2006).

[5] Pazokifard, B. and Sowmya, A., "3-D segmentation of human sternum in lung MDCT images," EMBC, 3351-3354 (2013).

[6] Lee, J., Reeves, A. P., Fotin, S. V., Apanasovich, T., et al., "Human airway measurement from CT images," Proc. SPIE 6915, 691518 (2008).

[7] Lee, J. and Reeves, A.P., "Segmentation of individual ribs from low-dose chest CT," Proc. SPIE 7624, 76243J (2010).

[8] Reeves, A. P., Biancardi, A. M., Yankelevitz, D. F., Fotin, S., et al., "A public image database to support research in computer aided diagnosis," EMBC, 3715–3718 (2009).

[9] Reeves, A. P., Biancardi, A. M., Apanasovich, T. V., Meyer, C. R., et al., "The lung image database consortium (LIDC) a comparison of different size metrics for pulmonary nodule measurements," Academic radiology 14(12), 1475-1485 (2007).